



A comparative investigation on self-piercing riveting and resistance spot welding of automotive grade dissimilar galvanized steel sheets

Brajesh Asati¹ · Nikhil Shajan¹ · Akhil Kishore V. T.² · Kanwer Singh Arora¹ · R. Ganesh Narayanan³

Received: 9 February 2022 / Accepted: 2 October 2022 / Published online: 10 October 2022
© The Author(s), under exclusive licence to Springer-Verlag London Ltd., part of Springer Nature 2022

Abstract

Self-piercing riveting (SPR) and resistance spot welding (RSW) are widely used spot joining methods in the automotive sector, with the former in developmental mode. The current work compares the joinability of dissimilar galvanized steels performed through SPR and RSW, which poses challenges during conventional RSW. Two widely used galvanized steels, CR340 and CR210, were selected for the study. SPR was optimized in terms of joint characteristics such as rivet head height, interlock distance, and remaining bottom sheet thickness. Similarly, a narrow optimal current range of 0.75 kA was optimized for RSW of steel sheets. Static and dynamic (fatigue) testing of joints was performed at optimized conditions and compared. RSW joints exhibited higher tensile-shear strength with greater scatter compared to SPR joints, whereas SPR joints showed significantly improved fatigue life. Different failure modes were observed for the two types of joints during fatigue life assessment. Failure mode for SPR joints subjected to cyclic tension-tension loading transitioned from rivet fracture to eyebrow cracking with decreasing applied loads, whereas RSW joints failed by eyebrow cracking at all load levels. Further, SPR joints suffered from fretting wear, whereas RSW joints showed poor dynamic performance owing to inherent geometrical notch.

Keywords Self-piercing rivet · Resistance spot welding · Galvanized steels · Mechanical performance · Dissimilar sheets joining · Failure modes

1 Introduction

Galvanized steel sheets are widely used in automotive industry with resistance spot welding (RSW) as the preferred joining process [1]. Galvanized steel sheets with zinc (Zn) coating are manufactured by hot-dip process, and the coating thickness is tailored to meet the corrosion performance [2]. While un-coated/bare steel sheets are easily spot welded, the coated galvanized steel sheets present significant challenges which require special attention to ensure consistent and reliable fabrication. Low electrical resistance and high

thermal conductivity of Zn coating necessitate higher welding current, higher electrode force, and longer weld time [3, 4], whereas reduced electrode life is a critical issue while joining hot dip galvanized steel sheets. Frequent dressing of electrodes also results in increased downtime and raised production cost. Self-piercing rivet (SPR) is a relatively new, alternate process for joining automotive-grade sheets. SPR is a mechanical joining process, and therefore, the above-mentioned issues related to Zn coating are eliminated [5]. But careful selection of rivet and die combination is critical and depends on stack thickness and material properties of sheets. Further, rivet head height (i.e., penetration) is to be optimized to achieve requisite mechanical properties and aesthetics [6].

Abe et al. [7] reported the importance of stack placement on the joining performance of SPR joints. The authors reported better SPR joint properties with harder steel on the top and softer aluminum sheet on the lower/die side. This was primarily due to two reasons: (a) the softer sheet ruptured during rivet piercing, when placed on the top but aids filling of the die and helps achieve the desired interlock while on the bottom side. Further, Ma et al. [8] studied the effect of rivet and die on joining of AA6061-T6 to mild steel

✉ Brajesh Asati
brajesh.asati@tatasteel.com; 0410brajesh@gmail.com

R. Ganesh Narayanan
ganu@iitg.ac.in

¹ Research and Development, TATA Steel Ltd., Jamshedpur, Jharkhand, India

² Department of Metallurgical and Materials Engineering, NITK, Surathkal, Mangalore, Karnataka, India

³ Department of Mechanical Engineering, IIT Guwahati, Guwahati, Assam, India

of different thickness. The author concluded that rivet hardness, rivet length, and die dimensions significantly affect rivetability, joint strength, and quality for the selected materials. Haque [9] reviewed quality of SPR joint with respect to joint geometrical features. The author reported that the joint quality primarily depends on mechanical interlocking (i.e., rivet flaring). Additionally, rivet head height, remaining bottom sheet thickness (T_{\min}), and rivet effective length in the bottom sheet also contributed to the joint quality. Han et al. [10] compared mechanical performance of aluminum joints prepared by SPR and RSW and concluded that although the tensile-shear strength of SPR was similar to RSW, the performance of SPR improved for thicker stack. Briskham et al. [11] compared the performance of SPR, RSW, and spot friction joining processes for automotive grade aluminum sheets and reported that SPR joints demonstrate superior mechanical properties. Uhe et al. [12] studied the effect of different rivets on static and dynamic performance of steel-aluminum SPR joints and found that, for steel-steel joints, traditional rivet and high nitrogen steel rivet result in comparable joint strength. However, for Al-steel joints, reduced joint strength is observed with high nitrogen steel rivet. Zhang et al. [13] evaluated the static and fatigue performance of steel-aluminum SPR joints and found that the thickness and strength of sheet material influenced joint tensile-shear strength and fatigue performance. Sun et al. [14] reported that fatigue strength for 2 mm 5182-O aluminum alloy SPR joints was approximately 100% higher compared to RSW joints. Booth et al. [15] evaluated tensile and fatigue properties of steel-steel and aluminum-aluminum joints of different thicknesses and reported that tensile-shear strength of RSW steel-steel joints was 25% higher than corresponding SPR joints, but the fatigue strength of SPR joints was better. The effect of friction on the SPR process and mechanical performance has been studied by researchers. Li [16] varied the surface texture of AA5754 to alter friction using hot water washing, sandpaper grinding, and grit blasting. Grit blasting increased the riveting force and altered the joint features due to change in frictional forces between the top and bottom sheet under the punched region. Static lap shear strength was found to be higher in grit blasting. Han and Chrysanthou [17] analyzed the effect of different coatings applied over aluminum-steel substrates and found that joint quality, joint strength, and failure modes are altered with the application of different coatings on the substrates. Uhe et al. [18] studied the effect of rivet coatings such as Almac, Zn–Ni on the friction and compared with uncoated rivets.

The surface coatings influence friction and the resultant joint quality. However, functional performance of SPR process is independent of the coating. Huang et al. [19] studied fatigue of steel-aluminum joints and observed fretting at the interface of steel-aluminum joints between rivet head and sheets which primarily contributed to crack initiation. Similarly, Han et al. [20] studied the effect of different interfacial conditions on fretting behavior of riveted aluminum alloy joints. The authors observed that fretting behavior and fatigue life are affected by interfacial condition, e.g., application of solid lubricant (wax-based). Li et al. [21] reported that the residual static strength of aluminum SPR joints increased for lap shear joints subjected to cyclic loading. They observed that fretting increased the frictional force between the sheets and subsequently improved static strength as load required to break the joint was combination of frictional and pull-out load.

Though a lot of literature are available on SPR, specific studies on advantages of SPR over RSW for difficult to weld dissimilar galvanized steels are few. In view of this, the present work aims to compare and understand the static and dynamic strength of SPR and RSW joints fabricated on galvanized steel sheets, CR340 and CR210, with different chemical composition and thicknesses. Further, microstructural changes during RSW, failure modes, and failure pattern during static and dynamic testing of SPR and RSW joints are also evaluated.

2 Materials and experiments

2.1 Materials

CR340 and CR210 galvanized steel sheets of 1.2-mm and 0.8-mm thicknesses with coating weight of 100 g were used to fabricate SPR and RSW joints. CR340 was kept as upper sheet, while CR210 as lower sheet. CR210 is an extra-low C (0.0019 wt. %) steel with Ti as the microalloying element, whereas CR340 has a higher C (0.045 wt. %) with Nb as the microalloying element. Chemical composition and mechanical properties of these steels are listed in Tables 1 and 2 respectively. Figure 1a, b shows the microstructure of as-received CR340 and CR210 steels. Both steels exhibit a fully ferritic microstructure. CR340 steel has a finer ferrite grain size compared to CR210 due to Nb microalloying addition. Figure 1c represents the engineering stress-engineering strain data evaluated from tensile tests as per ASTM E8 standard at

Table 1 Chemical composition (wt. %) of CR210 and CR340 steels

Base material	C	Mn	Al	Ti	Nb	Si	S	P	N (ppm)
CR210	0.0019	0.55	0.04	0.053	-	0.003	0.009	0.047	18
CR340	0.045	0.86	0.048	-	0.035	0.008	0.006	0.019	27

Table 2 Mechanical properties of CR210 and CR340 steels

Base material	Maximum load (kN)	Yield strength (MPa)	Tensile strength (MPa)	Elongation (%)	Strain hardening exponent	R_{avg}
CR210	3.46 ± 0.01	209 ± 2	334 ± 5	44 ± 0.8	0.21 ± 0.00	1.95 ± 0.16
CR340	6.51 ± 0.02	377 ± 3	431 ± 3	35 ± 0.2	0.19 ± 0.01	0.63 ± 0.03

a cross-head speed of 5 mm·min⁻¹. Maximum load bearing capacity of CR340 and CR210 were recorded as 6.51 kN and 3.46 kN respectively.

2.2 Specimen geometry and dimensions

Weld coupons measuring 105 mm × 45 mm for SPR and RSW joints were designed as per BS1140:1993 standard. Shims were welded at the grip section to minimize bending during tensile-shear tests. Figure 2b–d shows tensile testing

setup and photographs of tensile-shear specimens prepared by SPR and RSW.

2.3 SPR joint preparation

SPR joints were prepared using Tucker ERT 80 servo-electric system designed to deliver a maximum punch force of 80 kN. The selected semi-tubular boron steel rivets with the hardness of 480 ± 30 HV₁₀ possessed a countersunk head and Zn/Sn coating. The hardness of the rivet was sufficient to pierce the

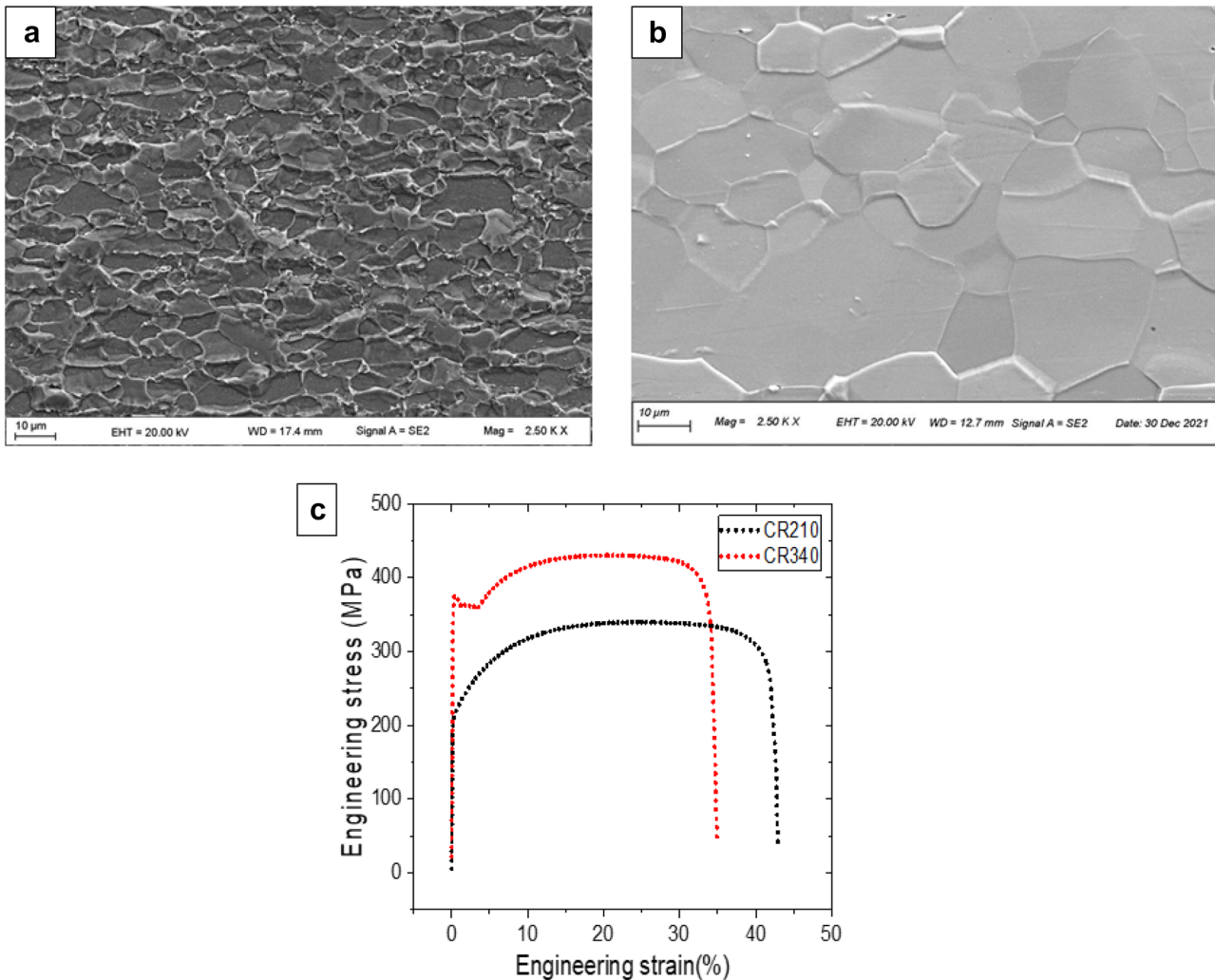


Fig. 1 Microstructure of **a** CR340, **b** CR210, and **c** engineering stress-engineering strain curves for CR210 and CR340 steels

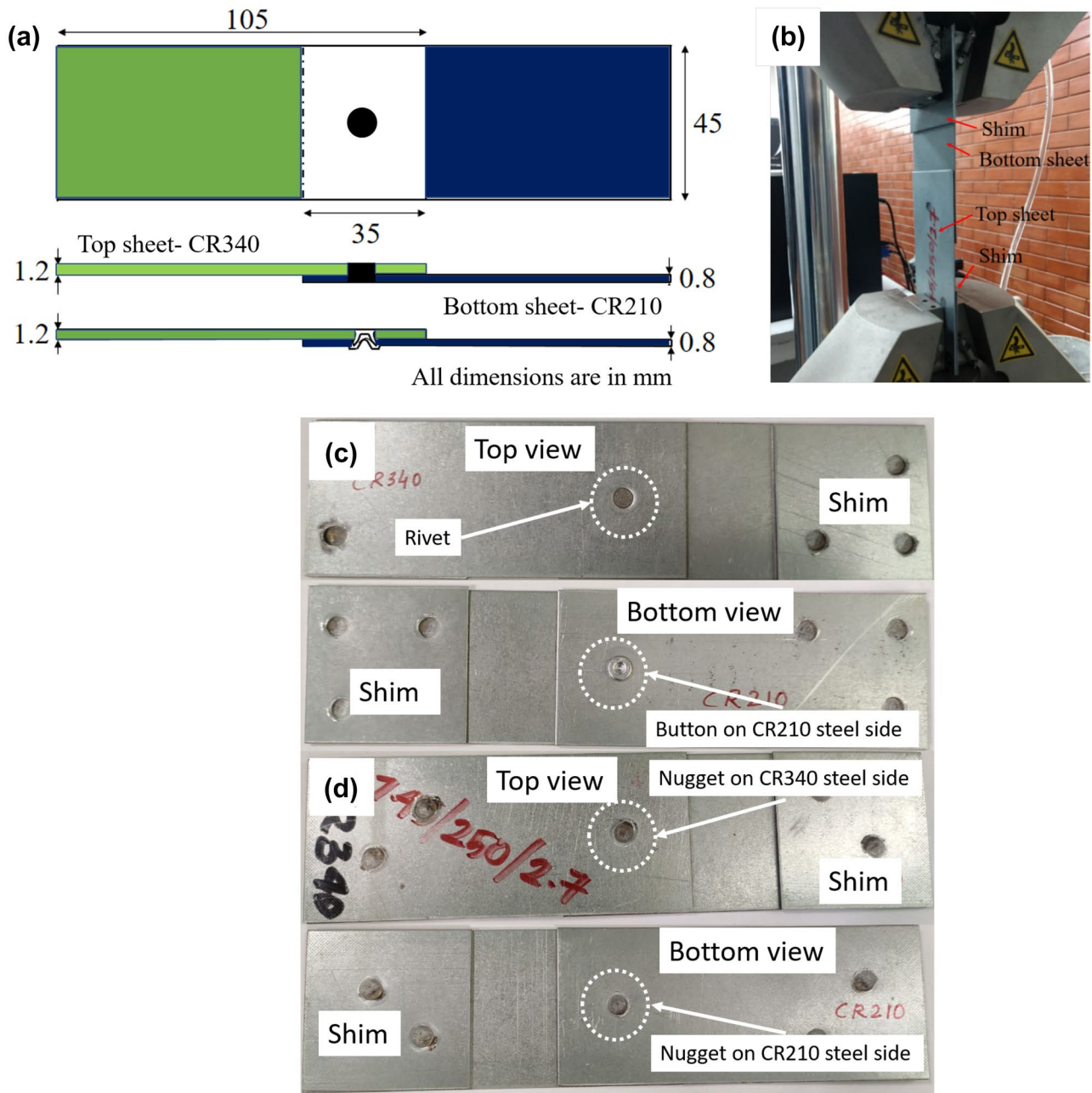


Fig. 2 **a** Joint design used for static tensile and fatigue tests in lap configuration. **b** Tensile-shear specimen gripped before testing. **c** CR340-CR210 SPR joint. **d** CR340-CR210 RSW joint

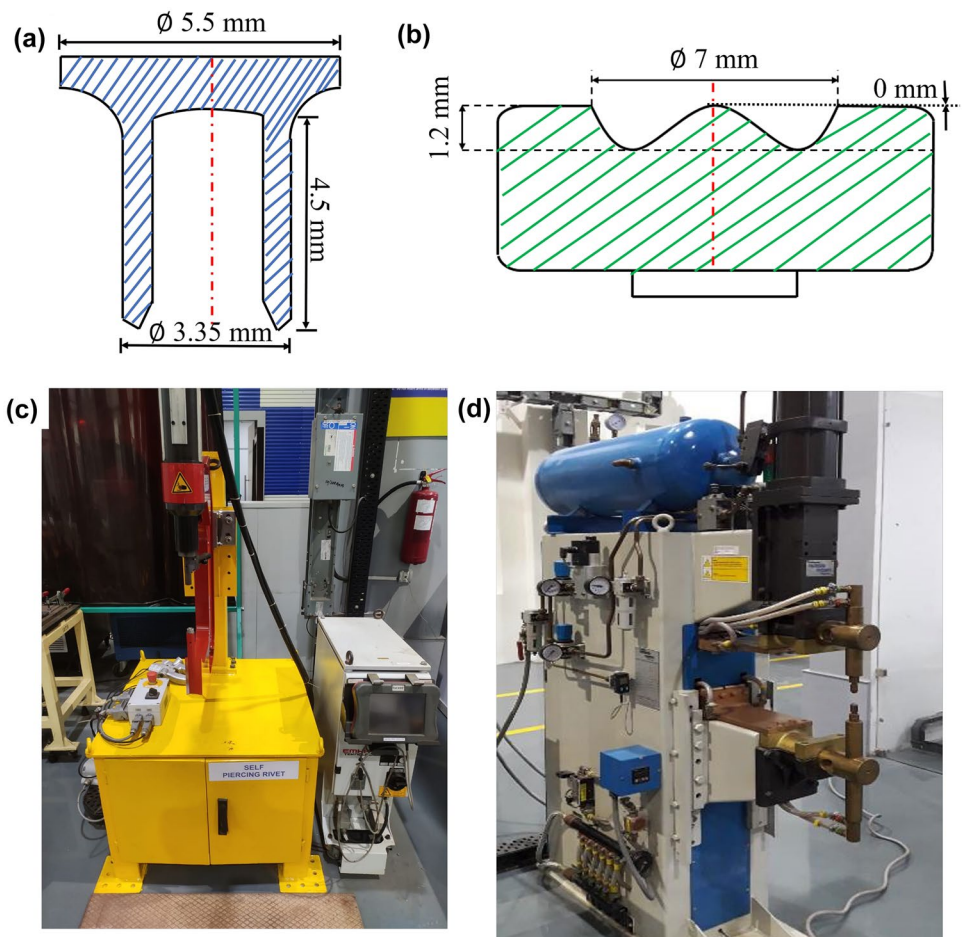
thicker/harder top sheet and to avoid buckling/compression. A pip die with a pip height of 0 mm was used during the experiments. Semi-tubular rivet and the pip die geometries and dimensional features are shown in Table 3 and Fig. 3a,

b. Desired head height (DHH) is optimized to ensure that the rivet head flushes with the top sheet surface within acceptable tolerance. For this study, SPR joints were manufactured with a DHH of -0.8 mm, and the actual head height (AHH) post

Table 3 Process parameters for SPR joint

Rivet	Die	Desired head height (DHH)	Riveting speed	Clamping force
3.35 mm × 4.5 mm, 480 HV	(D 070 120 000)	-0.8 mm	100 mm/s	2.5 kN

Fig. 3 **a** Semi-tubular rivet geometry, **b** pip die geometry, **c** SPR setup, and **d** RSW setup



riveting operation was measured using a Baker make height gauge. Riveted joints were sectioned, polished, and etched to reveal the cross section. AHH, interlock distance, and T_{min} were measured from the cross-sectional images.

2.4 RSW joint preparation

RSW was performed on a 150-kVA pedestal type medium frequency direct current (MFDC) machine (Fig. 3d) using 6-mm face diameter truncated cone shape Cu-Cr-Zr alloy electrode caps. Weld nugget growth curve was generated for a weld time of 250 ms and 2.7-kN electrode force. AWS recommended minimum critical nugget diameter of $4\sqrt{t}$, where “t,” which is the thickness of thinner sheet, was 3.57 mm, which is comparable to selected rivet shank diameter of 3.35 ± 0.15 mm, achieved at 7.45-kA welding

current. Further, expulsion was observed at 8.2 kA. Optimized RSW parameters are shown in Table 4.

2.5 Macro- and micro-structural examination, micro-hardness, fractography

For metallographic examination, joints were cut using a slow speed cutter, mounted, and polished to a mirror finish and examined under Leica M165C stereomicroscope, Leica DM6000M optical microscope, and Zeiss Supra 25 scanning electron microscope (SEM) for macrostructure, microstructure, and fractography studies. Micro-hardness measurement was performed using a Leco LM247AT Vickers microhardness tester. The applied load, dwell time, and indentation distance were 300 gf, 13 s, and 0.25 mm.

Table 4 Optimized RSW parameters

Weld current (kA)	Weld time (ms)	Electrode force (kN)	Squeeze time (ms)	Hold time (ms)	Coolant flow (L/min)	Face diameter (mm)	Shank diameter (mm)
7.45	250	2.7	600	200	4	6	16

2.6 Static and fatigue lap shear tensile tests

Lap shear tensile strength of SPR and RSW was determined using 250 kN Instron 5985 electromechanical system at a cross-head speed of 5 mm/min. A minimum of three samples were tested, and their average values with standard deviations are reported. Tension-tension fatigue tests with a load ratio $R (P_{\min}/P_{\max}) = 0.1$ were conducted using Instron ElectroPuls E10000 system at a frequency of 30 Hz. P_{\min} and P_{\max} indicate the minimum and maximum load applied during fatigue testing. P_{\max} was varied between 85 and 40% of the maximum static tensile-shear load for SPR and between 75 and 35% for RSW. This was done as to ensure that P_{\max} remained same for the two types of joints despite different static tensile-shear strength of SPR (3.95 ± 0.05 kN) and RSW (4.48 ± 0.33 kN). At least three samples were tested at each load level, i.e., 3.36 kN, 2.76 kN, 2.17 kN, and 1.58 kN, and cycles to failure were recorded with a run-out endurance limit of 5×10^6 cycles. Further, interrupted fatigue tests were conducted at pre-defined percentages of the average fatigue life (N_f) to analyze the fatigue crack initiation and growth mechanism for both SPR and RSW. Additionally, work hardening and the fretting behavior were examined for SPR during various stages of cyclic loading.

3 Results and discussion

3.1 SPR joint cross section

Figure 4 shows the macroscopic images of the cross section of SPR joints. Figure 4a shows the key joint characteristics, i.e., interlock distance (0.37 mm) and T_{\min} (0.45 mm) for a crack free joint. Insufficient interlock distance results in inferior mechanical properties. An optimal value of T_{\min} is significant so that the semi-tubular rivet does not puncture the bottom locked sheet [9]. Xu [22] reported that the interlock distance and T_{\min} value shall be greater than 0.2 mm to be acceptable as per standard industrial practice. Considering this, joint prepared in this work met the cross-sectional

quality requirement as reported in the literature. Rivet head height was ~ 0.03 mm, which indicates rivet head flushing with the top sheet and is important for avoiding crevice corrosion [23]. This was achieved by optimizing DHH at -0.8 mm, while an increase in DHH to -1.0 mm causes the rivet head to press into the top sheet and T_{\min} , in the center of the semi-tubular rivet reduced to near 0 because of gross compression of the thinner/softer CR210 sheet (Fig. 4b). Rao et al. [6] discussed the criticality of rivet head height as a vital parameter which influences both static and dynamic properties of SPR. Too high an indentation of rivet head into the top sheet reduces the tensile-shear load, and too low T_{\min} results in button cracks.

3.2 Current range and RSW joint cross section

Weld nugget variation with welding current, for constant electrode force of 2.7 kN and 250-ms weld time, is plotted in Fig. 5a. Nugget size increased with rising heat input ($H = I^2Rt$), as welding current is increased. Nugget diameter reached 3.57 mm equal to AWS recommended critical nugget diameter for 7.45 kA current. This is also comparable to semi-tubular rivet shank diameter of 3.35 ± 0.15 mm, whereas, expulsion was observed at 8.2 kA, which resulted in reduction in nugget diameter (Fig. 5a) since the molten metal is expunged out of the molten weld pool. Nugget diameter decreased from a peak value of 4.87 mm at 8 kA to 3.80 mm at expulsion current. Similar observation was made for HSLA-IF dissimilar steel spot welds by Janardhan et al. [24]. For RSW joints (Fig. 5b), an average nugget diameter of 3.57 mm was obtained for optimized welding conditions (i.e., weld time 250 ms, weld current 7.45 kA, and electrode force 2.7 kN).

CR340/CR210 weld nugget (Fig. 6a, b) exhibits a fully martensitic microstructure owing to the very high cooling rates experienced during RSW. Coarse grain heat affected zone (CGHAZ) of CR340 exhibits a fully martensitic microstructure (Fig. 6c) due to higher C content compared to a ferritic microstructure with a very low percentage of bainite for CR210 (Fig. 6d). Fine grain heat affected zone (FGHAZ)

Fig. 4 Cross section of SPR joints. **a** DHH: -0.8 mm; **b** DHH: -1.0 mm

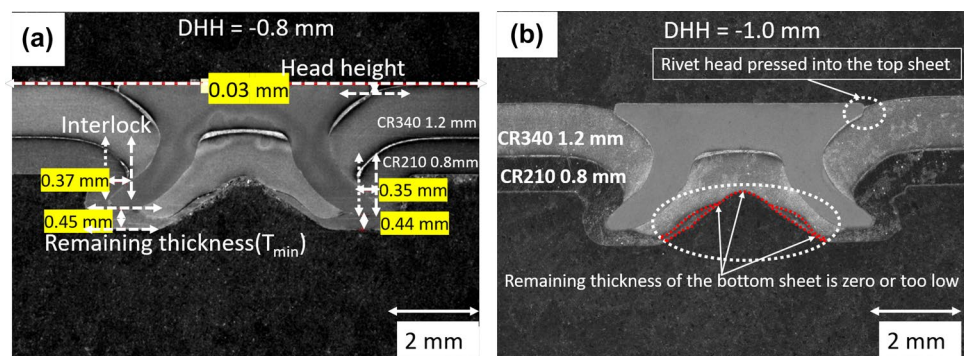
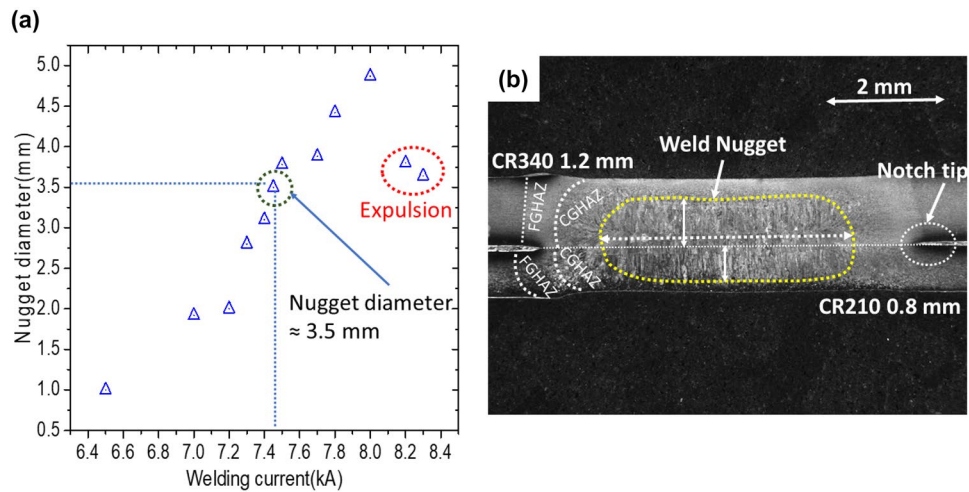


Fig. 5 a Variation of nugget diameter with increasing current in RSW. **b** Cross section of RSW joint at optimized welding current of 7.45 kA



of CR340 exhibits a fully martensite microstructure with shorter laths (Fig. 6e), primarily due to smaller prior austenite grain size which in turn is related to the lower peak temperature experienced in this zone, whereas CR210 shows an acicular microstructure in FGHAZ (Fig. 6f).

3.3 Static tensile-shear properties

RSW exhibited higher static tensile-shear strength of 4.48 kN as compared to 3.95 kN for SPR (Fig. 7a). Sun et al. [25] also observed similar results for dissimilar steel-aluminum joints. SPR showed less scatter (about 0.05 kN) compared to RSW (about 0.33 kN), which is in line with previous studies, e.g., Han et al. [10], wherein lower scatter was observed for SPR compared to RSW. Representative failure images of SPR and RSW are shown in Fig. 7b, c.

Larger scatter in RSW static tensile-shear strength is the result of variations in nugget diameter even for identical welding parameters (Fig. 8). Nugget diameter measured from failed samples exhibiting pull-out fracture (Fig. 7c) varied from a maximum of 5.49 ± 0.44 mm to a minimum of 3.25 ± 0.21 mm. Further, sample 4 showed interfacial fracture, and hence zero nugget diameter (Fig. 8). Further, tensile-shear strength was observed to increase with nugget diameter. The findings are in good agreement with Sawhill [26] who determined that for pull-out fracture, tensile-shear load of spot joints is directly proportional to nugget diameter.

During tensile-shear tests, riveted joints failed by interlock failure because of rivet pull-out from the bent thinner/softer CR210 (Fig. 7b). This indicates that the tensile-shear load exceeded the strength of the interlock achieved between the rivet and the CR210 bottom sheet. This finding is in agreement with previous findings that for thicker-thinner combination, tearing of the bottom sheet caused by interlock failure between the rivet and bottom sheet results in joint

failure [10, 27]. For RSW (Fig. 7c), variation in tensile-shear strength can be attributed to variation in nugget diameter. Nine out of 10 samples failed in desirable pull-out fracture mode with nugget pull-out from the thinner/softer bottom CR210 steel, whereas incomplete fusion resulted in interfacial failure mode (sample 4). Such load variations are a prime concern during RSW of galvanized steels, whereas SPR joints owing to the inherent process characteristics overcome this challenge.

3.4 Fatigue life of SPR and RSW joints

Figure 9a shows L-N curve for SPR and RSW joints. With decreasing maximum load, number of cycles to failure increased for both SPR and RSW. It is in good agreement with other researchers' findings involving fatigue life evaluation of dissimilar steels [28, 29]. As can be seen, SPR joints endured significantly higher cycles to failure compared to RSW joints, for all load levels. Endurance limit (5×10^6 cycles) for SPR joints was obtained for $P_{\max} = 1.58$ kN, whereas RSW joints endured 1,338,755 cycles at P_{\max} of 1.58 kN (35% of maximum RSW tensile-shear load). It is also concluded from Fig. 9 that SPR joints exhibited significantly high fatigue life compared to RSW joints at different percentages of maximum static tensile-shear load. Previous studies [10, 15, 25] which compared fatigue performance of SPR and RSW were mainly focused on Al or steel-Al joints, whereas open literature on fatigue performance comparison for SPR and RSW galvanized steels is rare. Comparative data of fatigue life for SPR and RSW joints has been shown in Fig. 9b. Tables 5 and 6 list cycles to failure and failure mode for cyclically loaded SPR and RSW joints.

Figure 10 shows the fractured samples of SPR and RSW joints after fatigue testing. At $P_{\max} = 3.36$ kN (85% and 75% of maximum static tensile-shear load for SPR and RSW respectively), RSW joints failed by tearing of the

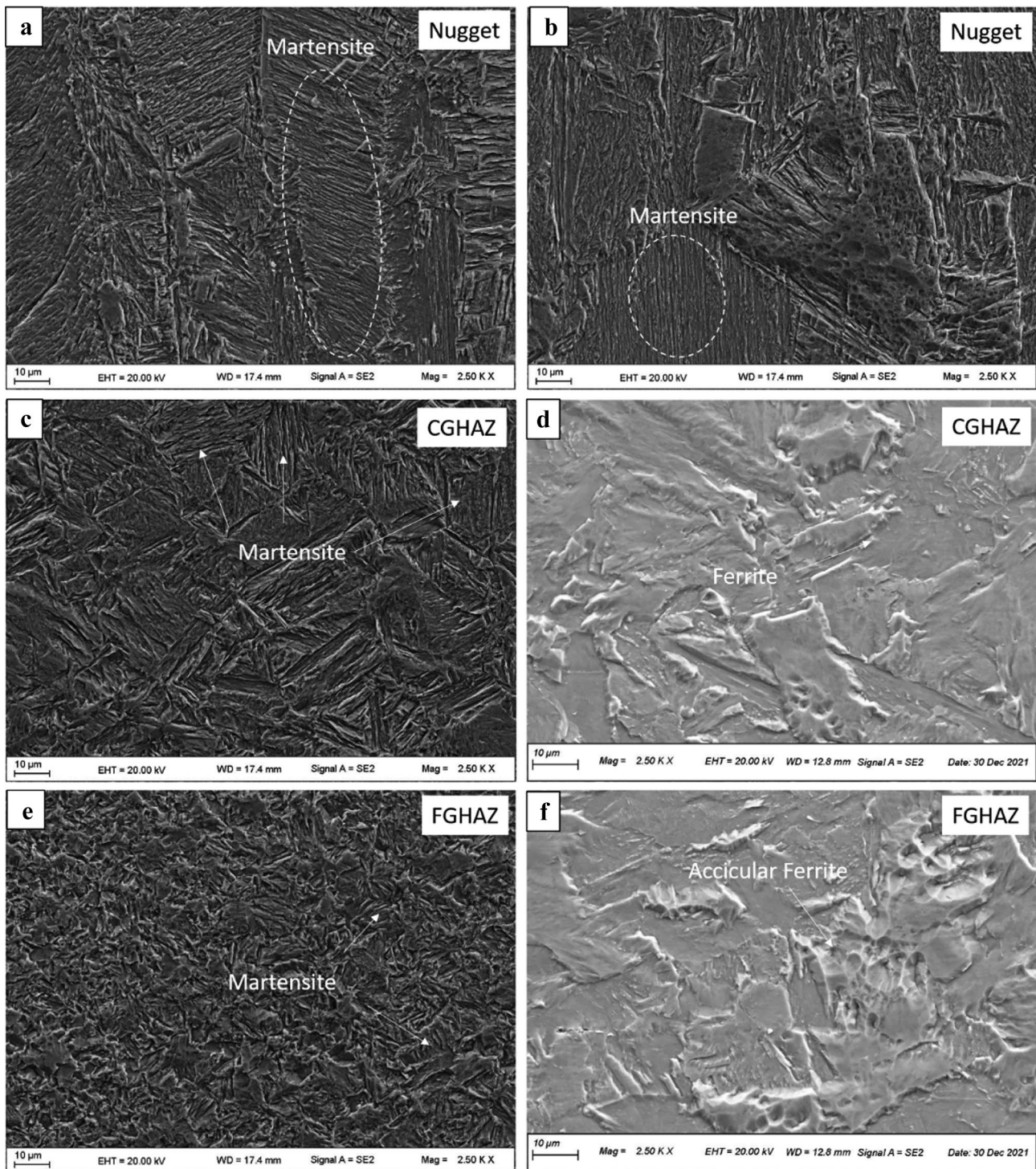
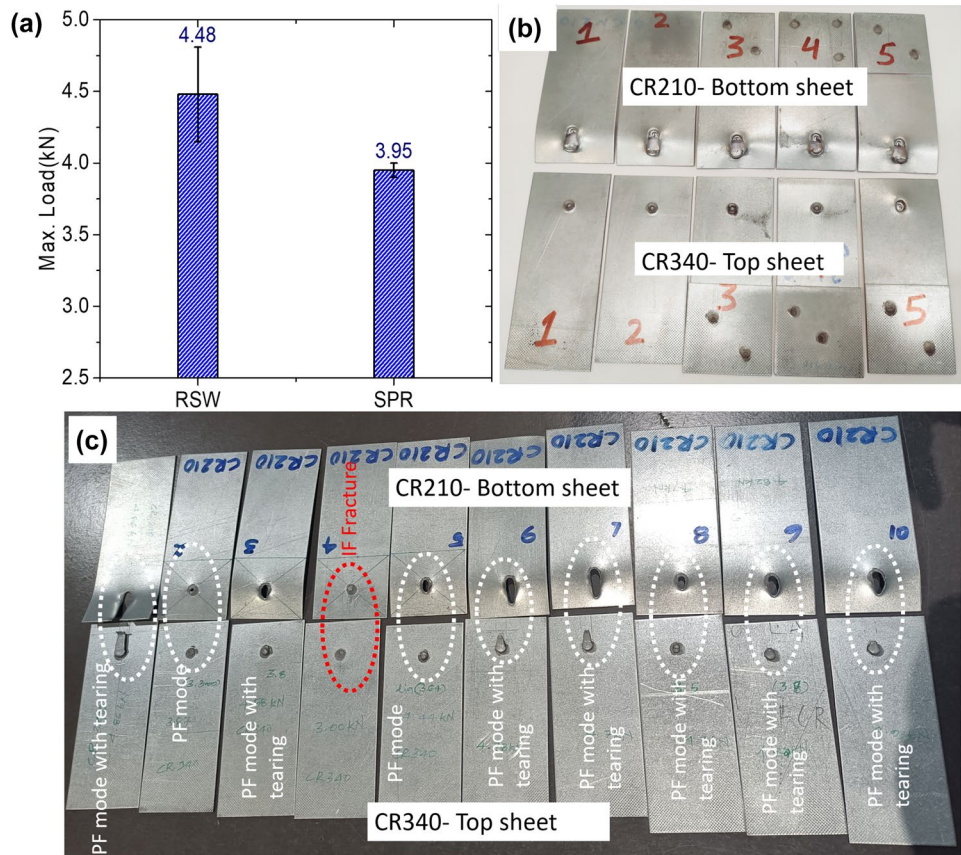


Fig. 6 Microstructure in different zones of RSW at optimized welding conditions. **a** Nugget of CR340, **b** nugget of CR210, **c** CGHAZ of CR340, **d** CGHAZ of CR210, **e** FGHAZ of CR340, **f** FGHAZ of CR210

thinner/softer CR210 sheet around weld nugget periphery, whereas corresponding SPR joints failed due to cracking of rivets. Fretting wear was also noticed between the sheets (Fig. 10b—region I). At $P_{\max} = 2.76$ kN (70% and

62% of maximum static tensile-shear load for SPR and RSW respectively), RSW joints failed by eyebrow crack formation along nugget periphery on thinner/softer CR210 sheet. Similar failure mode was observed by Janardhan

Fig. 7 **a** Static tensile-shear strength comparison of RSW and SPR joints, **b** representative images of SPR after static tensile-shear test, and **c** failure images of RSW after static tensile-shear test at optimized welding conditions



et al. [28] for dissimilar HSLA-IF spot welds. But corresponding SPR joints failed by a combination of eyebrow cracking in thicker/harder CR340 sheet around the rivet head and rivet fracture along with evidence of fretting wear. At $P_{max} = 2.17$ kN (55% and 48% of maximum

static tensile-shear load for SPR and RSW respectively). Similar failure mode was observed in RSW joints as for 2.76 kN sample; however, with decreasing maximum load and increasing cycles to failure, eyebrow crack length got increased. Further, SPR joints failed by similar eyebrow crack formation in CR340 steel (Fig. 10f) but no rivet fracture was noticed due to lower P_{max} . Fretting wear and a few cracks in the bottom CR210 sheet were observed. At $P_{max} = 1.58$ kN (40% and 35% of maximum static tensile-shear load for SPR and RSW respectively), RSW joints showed similar failure behavior as shown in Fig. 10g with eyebrow crack formation around nugget periphery in thinner/softer CR210 sheet, but the length of eyebrow crack was further increased due to decreased P_{max} and increased cycles to failure. As reported earlier, corresponding SPR joints did not fail, and the endurance limit of 5×10^6 cycles was achieved (Fig. 10h). RSW joints failed from thinner/softer CR210 sheet, but SPR joints failed from thicker/harder CR340 steel. It can also be inferred that thicker and harder sheet on top can help achieve superior fatigue performance since eyebrow crack initiates in top sheet at its interface with rivet head. Whereas RSW joints fail from the notch. Sun et al. [25] also listed the formation of notch tip and resultant stress concentration as the main reason for decreased fatigue life in RSW.

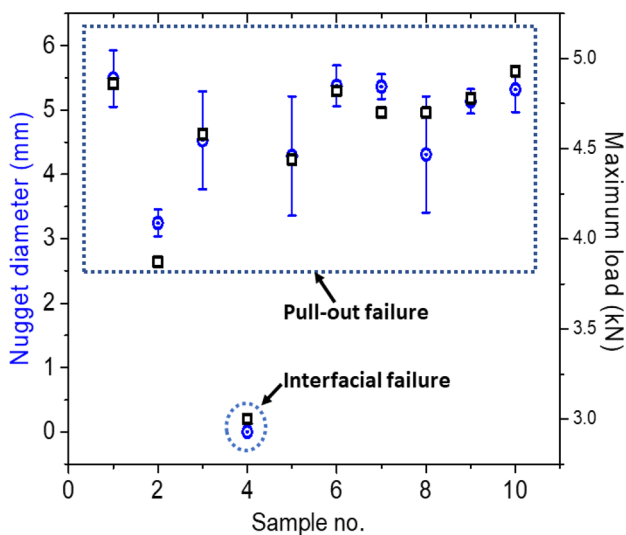


Fig. 8 Variation of nugget diameter and tensile-shear strength in ten RSW samples prepared at 7.45 kA

Fig. 9 **a** Fatigue curve for SPR and RSW joints, **b** comparative data of fatigue life for SPR and RSW joints

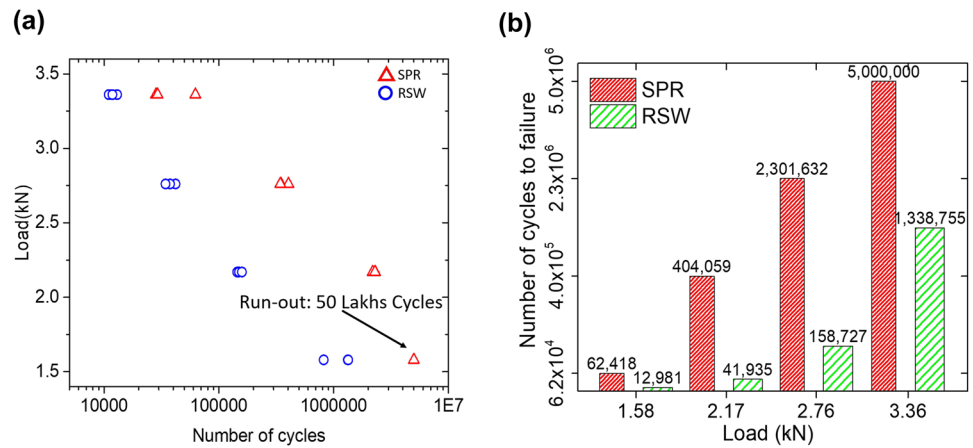


Table 5 Maximum load, number of cycles to failure, and failure mode for SPR joints

% of maximum tensile-shear load	Maximum load (kN)	Number of cycles			Failure mode
		Sample 1	Sample 2	Sample 3	
85	3.36	62,418	28,362	29,244	Rivet fracture
70	2.76	347,767	404,059	343,505	Rivet fracture and eyebrow crack in CR340 steel
55	2.17	2,301,632	2,188,972	2,292,472	Eyebrow crack in CR340 steel
40	1.58	5,000,000*	5,000,000*	5,000,000*	*Run-out

*indicates run-out condition i.e. 50 lakhs fatigue cycles without any visible crack

3.5 Failure analysis of SPR and RSW joints

SPR joints failed by either eyebrow cracking, rivet fracture, or by a combination of both. For low P_{max} load, failure was primarily through eyebrow cracking, whereas, at higher P_{max} load, rivet failure was observed. Similar findings were also reported by Huang et al. [19] for dissimilar Al/steel SPR joints. At low loading levels, eyebrow cracks were prominent; however, at high load, rivet fracture was observed. SEM analysis of fracture surface of eyebrow crack in SPR joint (Fig. 10f), which failed after 2.3 million cycles at $P_{max} = 2.17$ kN, is shown in Fig. 11. Figure 11a shows the cross section of eyebrow crack. Faying surface is on the top side of the image, with the top surface of CR340 steel marked as “S.” Fracture surface (Fig. 11b) depicts the river marks emanating from the crack initiation point indicating the direction of fatigue crack growth. This is in good

agreement with the findings of Huang et al. [30]. Similar fracture mechanism of eyebrow crack formation in the top sheet with river marks initiating from the center of the plate width is observed.

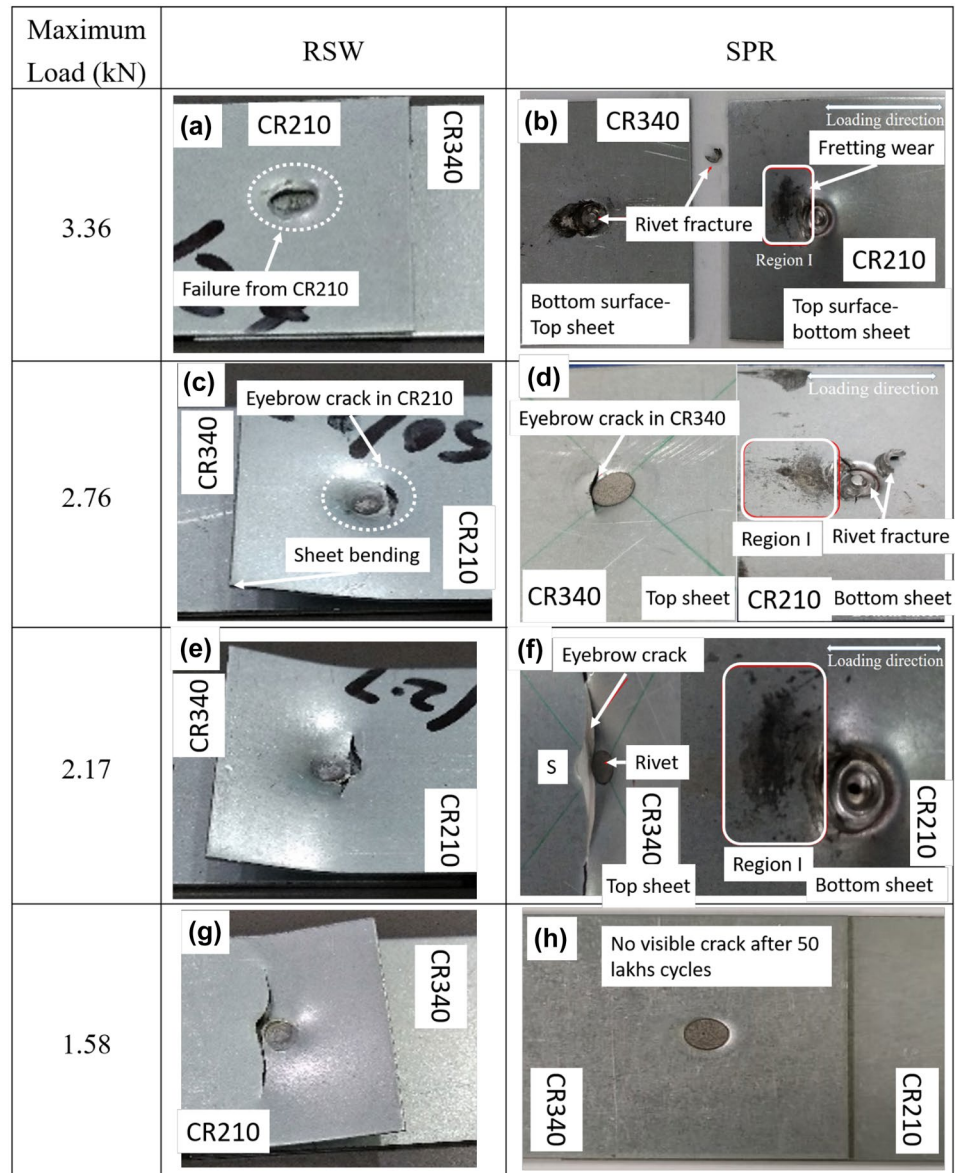
Another prominent mode of failure observed in SPR joints was rivet fracture. To capture the failure mechanism, SPR joints failed at 2.76 kN and 347,767 fatigue cycles as shown in Fig. 10d were examined in SEM. This sample failed by combined eyebrow crack in the top sheet and rivet fracture (Fig. 12a). Fracture surface of the sheared rivet leg shows dimples indicating ductile fracture (Fig. 12b). Figure 12c shows the magnified view of region I as shown in Fig. 12a. Fatigue cracks are also observed on the bottom sheet as striations mark is visible in Fig. 12d.

Figure 13a, b shows schematics of fatigue loading and fretting regions of a SPR joint. Tensile loads act in opposing direction on the top and bottom halves of the rivet, which

Table 6 Maximum load, number of cycles to failure, and failure mode for RSW joints

% of maximum tensile-shear load	Maximum load (kN)	Number of cycles			Failure mode
		Sample 1	Sample 2	Sample 3	
75	3.36	10,990	12,981	11,829	Nugget pull-out from CR210 sheet
62	2.76	41,935	37,582	34,276	Eyebrow crack on the periphery of the nugget in CR210 sheet
48	2.17	144,529	149,767	158,727	Eyebrow crack on the periphery of the nugget in CR210 sheet
35	1.58	819,155	1,329,343	1,338,755	Eyebrow crack on the periphery of the nugget in CR210 sheet

Fig. 10 Fatigue failure samples of RSW and SPR at different load levels



tilts the rivet by a small angle. This tilting of the rivet due to eccentric loading is termed as secondary bending. Further, tilting the rivet causes an increase in friction between the two sheets—region I and the rivet presses against the top sheet—region II (Fig. 13b). The combined effect of secondary bending and fretting wear results in eyebrow cracking [27, 30]. Burnt marks are also observed on sheets where friction was more due to secondary bending.

Failure mode changed from eyebrow cracking (Fig. 10f) to rivet fracture (Fig. 10b, d) at higher load levels. Failure mechanism in this case is a combined effect of fretting and shearing. As shown in Fig. 13a, fretting occurs on the outer surface near the rivet leg tip. In addition to this, since the rivet was made of boron steel having yield strength more than 1500 MPa, rapid fracture zone observed in Fig. 12b indicates the crack sensitive nature of this steel [19].

To ascertain elemental distribution of the fretting debris, region I, marked in Fig. 13b, was analyzed using SEM/EDS. Researchers [31–35] have suggested that the fretting is more prominent in the region I. As evident in Fig. 14, the debris was mainly oxides of zinc and iron. Galvanized steel has Zn coating, which is removed during repeated cyclic loading due to rubbing of sheets and Fe of steel was exposed and oxidized. The removal of Zn coating from coated steels can accelerate corrosion during service.

Figure 15 shows the failure analysis of RSW joints. Intermittent fatigue tests were conducted to study the crack initiation and crack growth mechanism. RSW joints failed by eyebrow cracking in HAZ of thinner/softer CR210 steel. Figure 15a, b shows optical images of the crack occurred in HAZ of CR210 steel at different magnifications. Presence of notch along nutget circumference results in stress

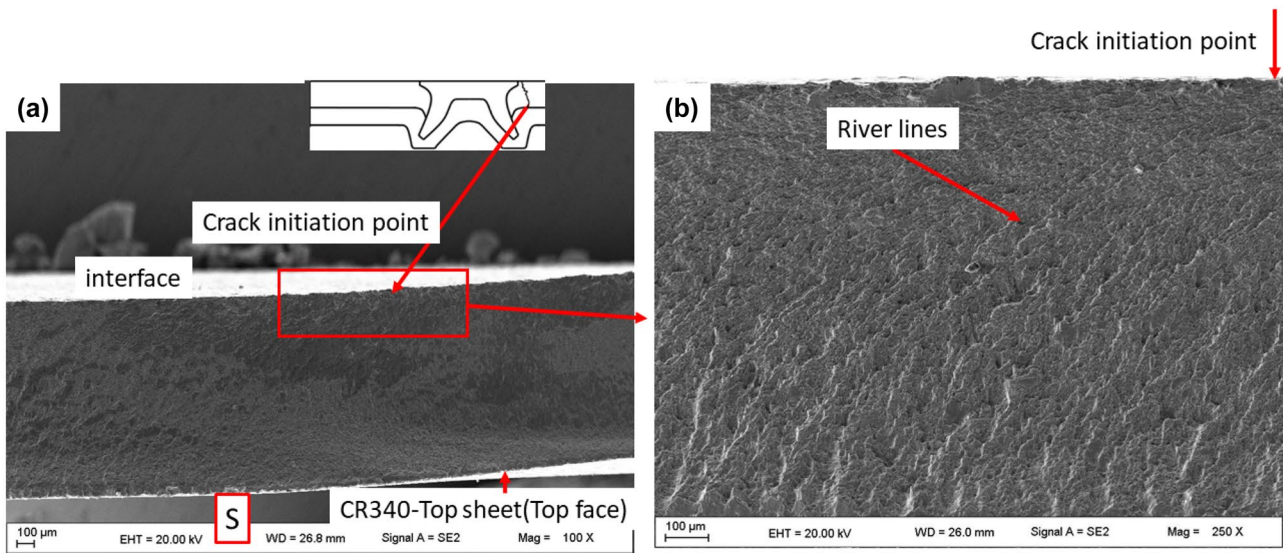


Fig. 11 SEM images of fatigue sample failed at 2.17 kN. **a** Crack initiation point, **b** river lines

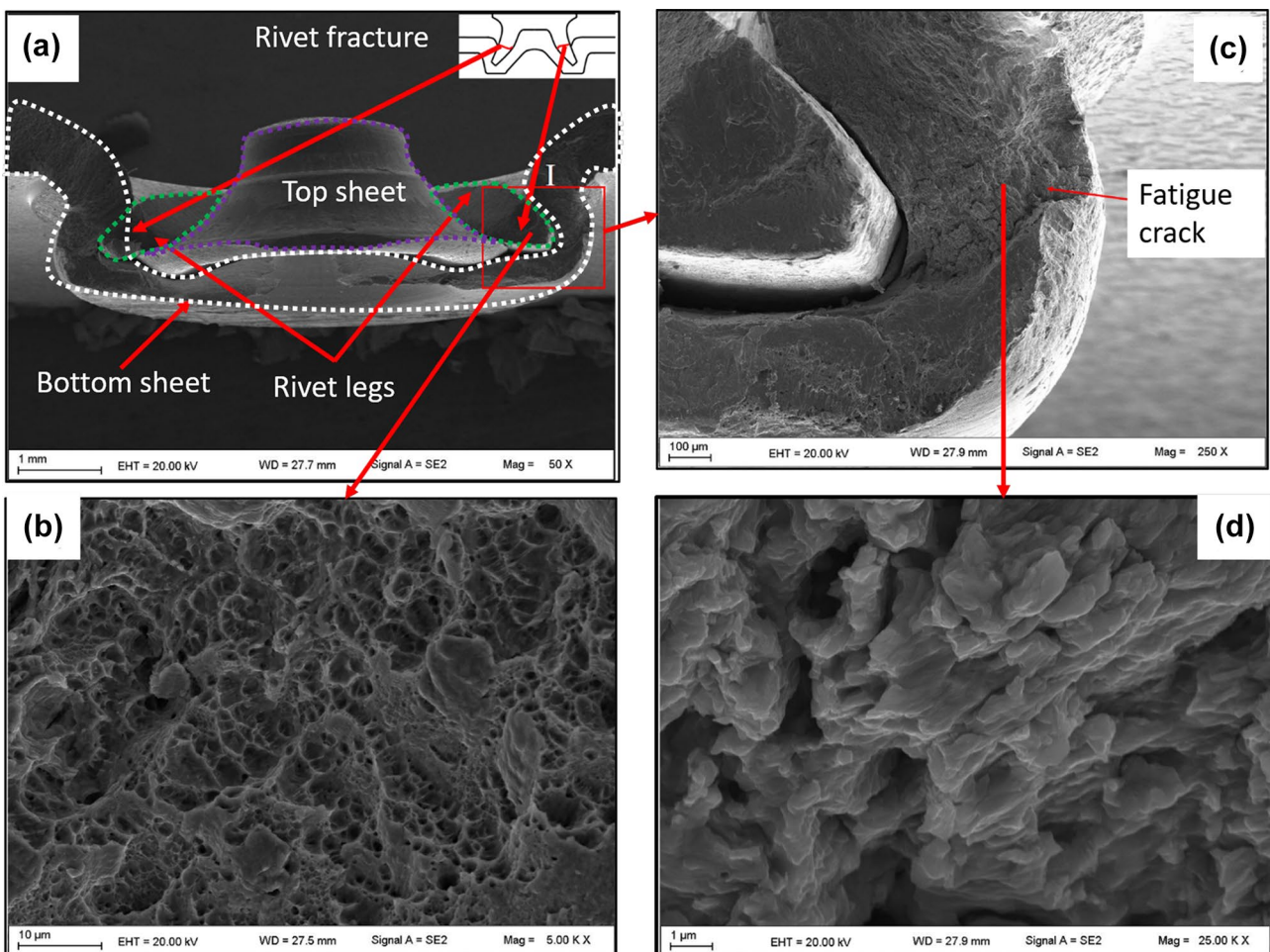
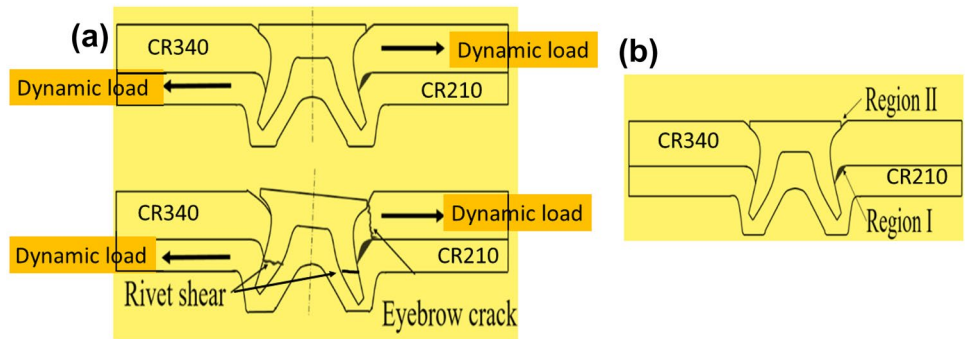


Fig. 12 Fatigue fracture surface failed at 2.76 kN. **a** Cross-sectional view, **b** fracture surface of the rivet leg tip, **c**, **d** fatigue cracks and striations marks observed on the bottom CR210 steel

Fig. 13 **a** Schematic of fatigue loading, **b** schematic of fretting regions in SPR joints



concentration, which deteriorates fatigue performance of RSW compared to SPR. Previous studies [28, 29, 36] have also highlighted the deleterious effect of notch as crack initiation region. Figure 15c, d shows SEM images of cracked spot weld cross section at different magnification. Figure 15e shows a SEM image of fracture surface of bottom CR210 sheet with river marks initiated from the faying surface indicative of crack initiation point. Hardness measurement was performed across weld nugget in both steel sheets (Fig. 16a, b). For CR210 steel, hardness values in base material (BM), HAZ, and nugget were recorded as 115 ± 6 HV, 188 ± 16 HV, and 307 ± 5 HV respectively. For CR340 steel, corresponding values were 156 ± 8 HV, 316 ± 43 HV, and

297 ± 3 HV respectively. Crack initiation and propagation occurred, perpendicular to the loading direction, in HAZ of CR210 steel where the hardness is significantly less compared to the adjacent CR340 HAZ. Previous literature on dissimilar steels spot welding [28, 29] also reported fatigue failure in the softer of the two steels. Weld nugget hardness is similar in the nugget formed on both the sides indicating good chemical homogeneity in the weld zone. Lower hardness in the HAZ of CR210 steel is primarily due to ferrite/acicular ferrite microstructure compared to harder martensite phase on HAZ of CR340. Khan et al. [37] observed similar failure for dissimilar DP/HSLA steels spot welds, where failure occurred from HAZ of HSLA steel.

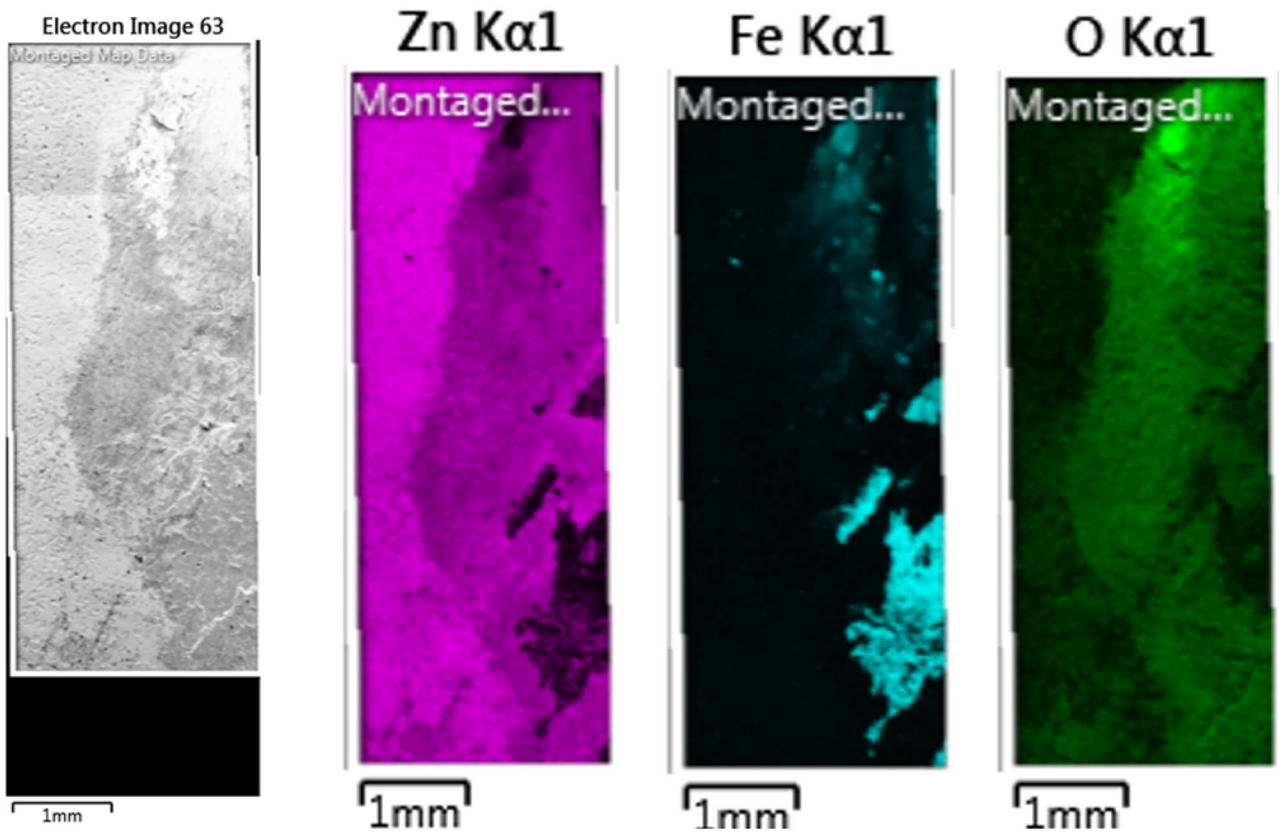


Fig. 14 SEM/EDS maps representing the fretting debris

Fig. 15 **a, b** Optical images of the crack, **c, d** SEM images of the crack, **e** fracture surface of RSW sample after intermittent fatigue test

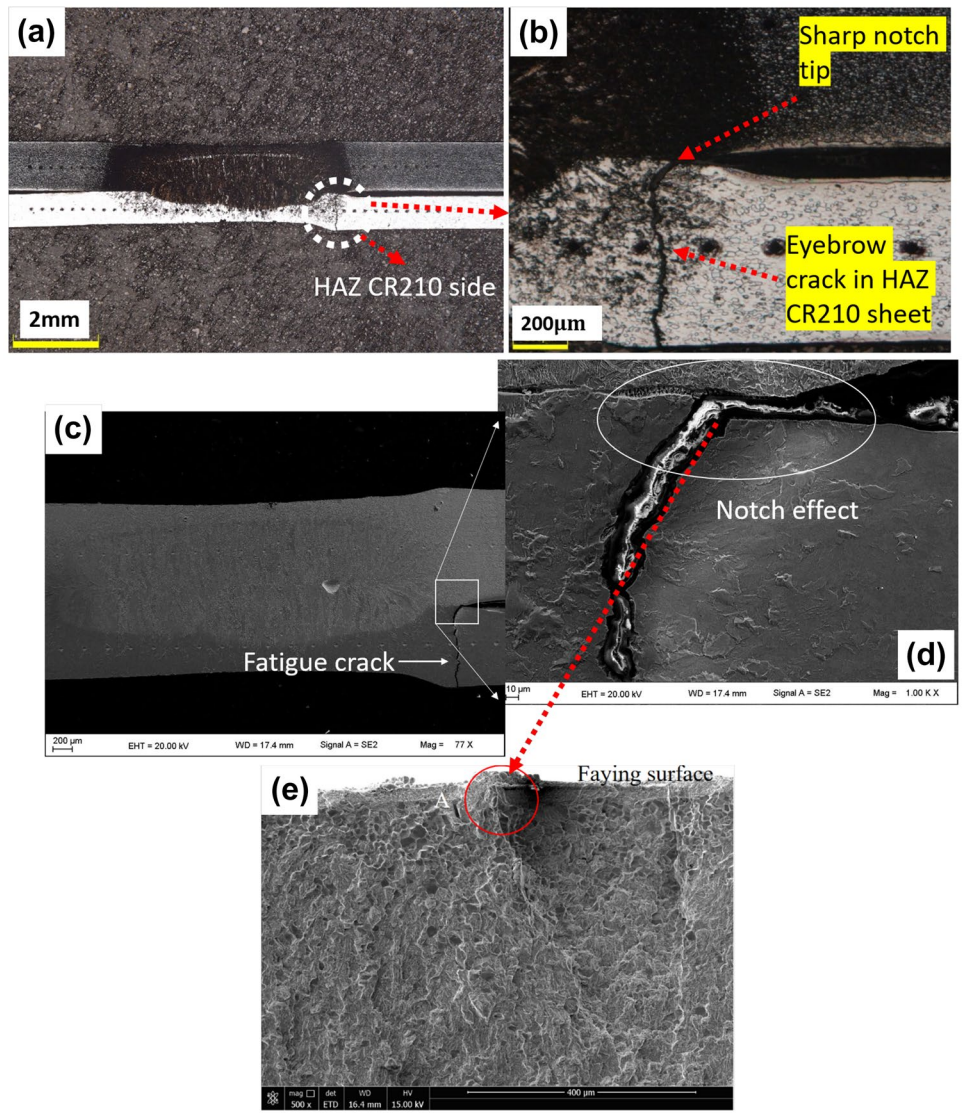
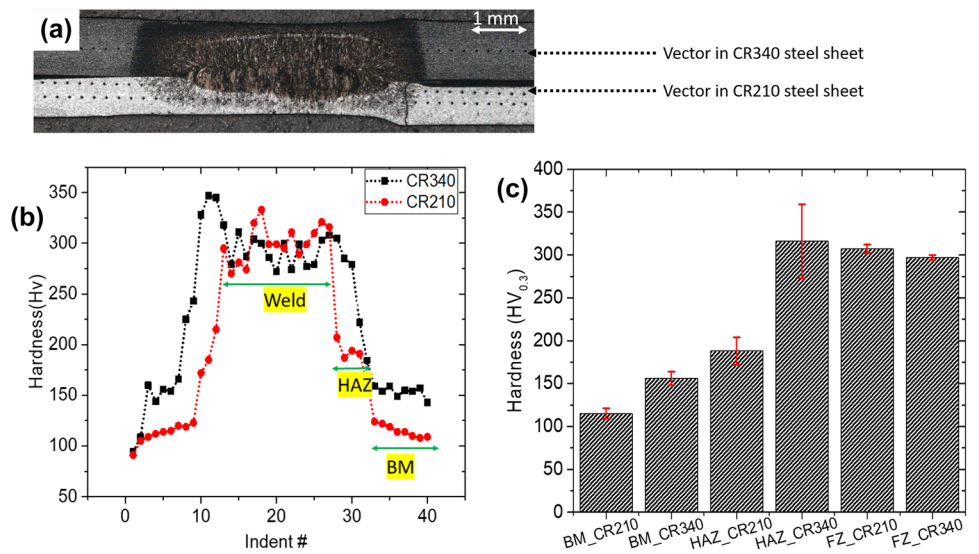


Fig. 16 Micro-hardness measurement in spot weld after intermittent fatigue test. **a** Macro-image with indentation points, **b** micro-hardness in different zones, **c** comparison of micro-hardness in different zones of CR210 and CR340 steels



3.6 Various reasons for improvement in fatigue performance of SPR over RSW

Superior fatigue performance of SPR and transition in failure mode with decreasing load made an intriguing case for evaluation of residual tensile-shear strength, i.e., strength after pre-defined fatigue cycles for these joints. All RSW joints failed in the same manner along HAZ of thinner/softer CR210 steel, with crack initiating from the inherent geometrical notch, a high stress concentration zone. Therefore,

residual tensile-shear strength was not determined for spot welds. Figure 17a shows residual tensile-shear strength of SPR joints subjected to cyclic tension-tension loads for pre-defined number of cycles at different P_{max} values, i.e., 2.77 kN, 2.17 kN, and 1.58 kN. Residual tensile-shear strength was observed to be greater than the initial strength of joints. For 50% of N_f values, residual tensile-shear strength was observed to decrease with P_{max} value, whereas, for a selected P_{max} values residual tensile-shear strength was greater for sample subjected to greater number of loading cycles.

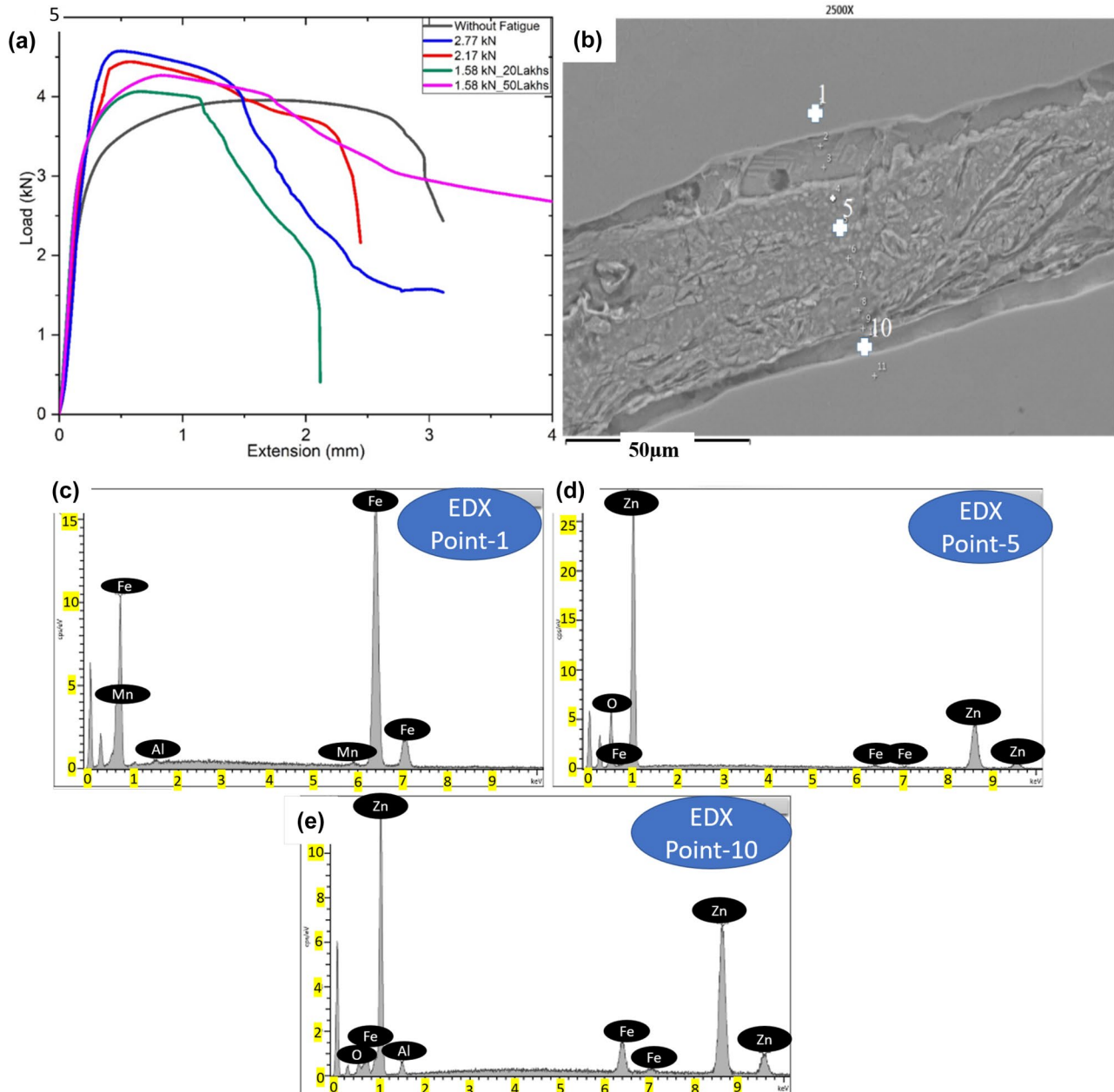


Fig. 17 Static tensile-shear after fatigue in SPR joints. **a** Load-extension curve, **b** SEM image of the interface of CR340-CR210 joint, **c-e** elemental distribution at the interface

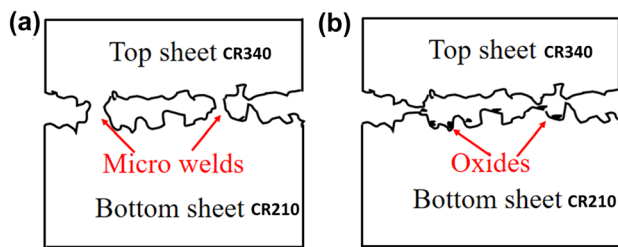


Fig. 18 Schematic of **a** micro-welds formation, **b** fretting debris in SPR joints during fatigue testing

Figure 17b shows the SEM image with EDX analysis points in region 1 marked in Fig. 13b. EDX maps of Point 1 (i.e., CR340), 5, and 10 (i.e., interface) are shown in Fig. 17c–e respectively. Elements of EDX point 1 represent CR340 steel chemical composition, whereas EDX points 5 and 10 show Zn as the major element, present in the oxide form on the interface, as this region experiences higher frictional heat. Zn has a low melting point of 419 °C and melts due to frictional heat caused by rubbing of sheets, which is the combined effect of rivet tilting and repetitive loading during fatigue tests.

This results in micro-welds at the interface, hindering rivet pullout and subsequently improving load bearing ability of SPR joint during fatigue. Kaneko and Sasaki [38] explained the formation of partially bonded regions due to Zn melting during ultrasonic spot welding of galvanized steels and subsequent increase in strength. They explained that the weld formation occurred in two steps. Initially, Zn coating at the interface was mechanically detached by the vibration and holding force, and some Zn elements distributed at the joint interface. Subsequently, the Zn particles dissolved owing to the friction, and moderately fused areas were concurrently formed around the Zn particles. The moderately fused regions were mixed with the steel base sheet as the weld time was increased. The joint strength further enhanced by expansion of the mixed zone. In ultrasonic spot welding, vibrational frequency is typically 20 kHz, and the weld time is around 1.0 s, which means just about 20,000 vibration cycles can spot weld the galvanized steel sheets and improve the joint strength. On the contrary, in case of fatigue testing of SPR joints, despite low frequency of 30 Hz, the number of vibration cycles (loading–unloading) and the associated completion time are quite high. For, e.g., 5 million cycles

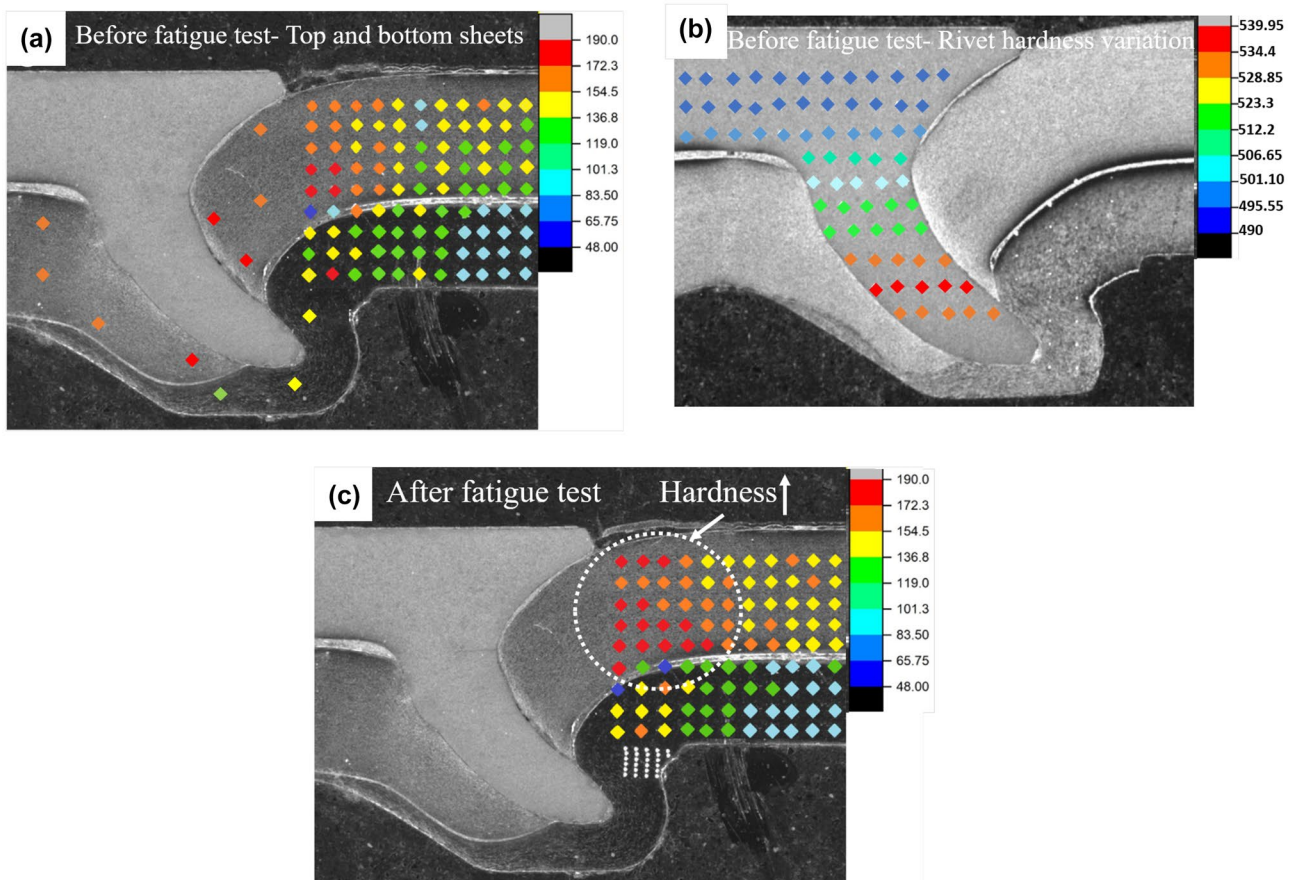


Fig. 19 Microhardness profile, **a** before fatigue test in top and bottom sheets, **b** before fatigue test in rivet, **c** after fatigue test (i.e., 2.76 kN, 1.1 million cycles) in top and bottom sheets

will need vibration time of 46.29 h at a frequency of 30 Hz. Vibrations introduced during high cycle fatigue experiments coupled with fretting of the galvanized steel sheets in SPR will naturally cause temperature rise leading to Zn melting and formation of micro-welds resulting in increased residual static tensile-shear strength (Fig. 17a) as explained by Kaneko and Sasaki [38]. Increased residual static tensile-shear strength will improve the fatigue performance.

At higher loads, fretting debris amount increased because of higher frictional heat and formation of micro-welds at the interface. Increase in coefficient of friction results from debris formation which acts as third body micro particles [31]. Subsequently, fatigue life of SPR joints improves as a portion of applied load is transferred through micro-welds between sheets rather than directly bearing on the rivet. The micro-welds and micro particles (i.e., fretting debris) formations are schematically represented in Fig. 18. Figure 19a–c represents the microhardness profile of the SPR joint before and after fatigue test at $P_{\max} = 2.77$ kN and 182,000 cycles. Micro-hardness increased from 150 to 190 HV (about 40 HV increment) near the fretting region, i.e., region II of Fig. 13b primarily due to surface hardening. Han et al. [34] also observed that fretting resulted in hardness improvement due to surface work-hardening for 5754 aluminum alloy riveted joints subjected to high cycle fatigue. Rivet hardness varied from 490 to 540 HV starting from rivet head to rivet leg tip, which is due to strain hardening of rivet leg during sheet piercing and flaring.

4 Conclusions

The main aim of the current work is to compare and understand the static and fatigue performance of SPR and RSW joints fabricated on CR340 and CR210 galvanized steel sheets of 1.2 mm and 0.8-mm thicknesses. The following conclusions are drawn from the results obtained.

1. CR340-CR210 SPR joints showed lower tensile-shear strength compared to RSW joints for similar shank/nugget diameter ≈ 3.5 mm. However, RSW joints showed greater scatter compared to SPR joints primarily due to the variation in nugget size for galvanized steels.
2. During static tensile-shear strength test, RSW joints failed with nugget pull-out from the thinner/softer CR210 steel, and SPR joints failure was combination of the rivet pull-out and button fracture of thinner/softer CR210 steel.
3. Fatigue performance of SPR joints was significantly higher than the RSW joints for various load levels set at defined percentages of maximum static tensile-shear load.
4. For RSW process, HAZ on CR340 steel showed higher hardness owing to harder martensitic microstructure and

failure crack always propagated through HAZ of thinner and lower strength CR210 steel with acicular ferrite microstructure.

5. Different fatigue failure modes were observed for RSW and SPR joints. In RSW, eyebrow cracking in HAZ of thinner/softer CR210 steel initiated from sharp notch tip, whereas, for SPR joints, either eyebrow cracking / rivet fracture or combination of both was observed at different loading levels. However, eyebrow crack formation was observed in the thicker/stronger CR340 steel contrary to RSW joints. Better fatigue performance observed in the SPR joints is influenced by the predominant failure observed in thicker/stronger CR340 steel.
6. Residual static tensile-shear strength after pre-defined fatigue cycles increased in SPR joints. As the static tensile strength of the joints increases, fatigue strength also improves. Increase in static tensile-shear strength can be attributed to (a) increase in coefficient of friction, (b) increase in hardness near the fretting region, and (c) formation of micro-welds.
7. An unfavorable narrow current range of 0.75 kA (7.45 to 8.2 kA) was observed for RSW, which can lead to inconsistent weld performance in service. Inconsistent nugget formation was also observed since the heat generated during RSW depends on the resistance, which varies with coating inconsistency. More heat generation in CR340 steel led to larger fusion zone compared with CR210 steel.

Acknowledgements The authors would like to thank Tata Steel's Welding Research Center support staff for their help in performing the experiments.

Author contribution BA, KSA, NS, and RGN formulated this work and outlined experiments; BA, AKVT, and NS performed the experiments; data collection was done by BA, AKVT, and NS; microstructural examinations were done by NS, AKVT, and BA. Data analysis was done by BA, NS, and AKVT; BA, NS, AKVT, KSA, and RGN wrote the paper and participated in the revisions of it. All authors scrutinized and approved the final manuscript.

Availability of data and material The datasets analyzed during this research are available from the corresponding author to the extent possible.

Code availability Not applicable.

Declarations

Consent to participate Not applicable.

Consent for publication Not applicable.

Conflict of interest The authors declare no competing interests.

References

- Gou R-B, Dan W-J, Zhang W-G (2016) Influence of spot welding on welding fatigue properties of CR340 steel joints. *J Iron Steel Res Int* 23(8):822–827. [https://doi.org/10.1016/S1006-706X\(16\)30126-1](https://doi.org/10.1016/S1006-706X(16)30126-1)
- Ghalib L, Muhammad AK, Mahdi SM (2021) Study the effect of adding titanium powder on the corrosion behavior for spot welded low carbon steel sheets. *J Inorg Organomet Polym Mater* 31(6):2665–2671. <https://doi.org/10.1007/s10904-020-01863-5>
- Lin HC, Hsu CA, Lee CS, Kuo TY, Jeng SL (2018) Effects of zinc layer thickness on resistance spot welding of galvanized mild steel. *J Mater Process Technol* 251:205–213. <https://doi.org/10.1016/j.jmatprotec.2017.08.035>
- Feujofack Kemda BV, Barka N, Jahazi M, Osmani D (2019) Optimization of resistance spot welding process applied to A36 mild steel and hot dipped galvanized steel based on hardness and nugget geometry. *Int J Adv Manuf Technol* 106(5–6):2477–2491. <https://doi.org/10.1007/s00170-019-04707-w>
- Tang D, Evans M, Briskham P, Susmel L, Sims N (2021) Dynamic modelling of a servo self-pierce riveting (SPR) process. *Proc Inst Mech Eng B J Eng Manuf* 235(13):2052–2065. <https://doi.org/10.1177/09544054211037493>
- Rao HM, Kang J, Huff G, Avery K, Su X (2017) Impact of rivet head height on the tensile and fatigue properties of lap shear self-pierced riveted CFRP to aluminum. *SAE Int J Mater Manuf* 10(2):167–173. <https://doi.org/10.4271/2017-01-0477>
- Abe Y, Kato T, Mori K (2009) Self-piercing riveting of high tensile strength steel and aluminium alloy sheets using conventional rivet and die. *J Mater Process Technol* 209(8):3914–3922. <https://doi.org/10.1016/j.jmatprotec.2008.09.007>
- Ma Y, Lou M, Li Y, Lin Z (2018) Effect of rivet and die on self-piercing rivetability of AA6061-T6 and mild steel CR4 of different gauges. *J Mater Process Technol* 251:282–294. <https://doi.org/10.1016/j.jmatprotec.2017.08.020>
- Haque R (2018) Quality of self-piercing riveting (SPR) joints from cross-sectional perspective: A review. *Arch Civ Mech Eng* 18(1):83–93. <https://doi.org/10.1016/j.acme.2017.06.003>
- Han L, Thornton M, Shergold M (2010) A comparison of the mechanical behaviour of self-piercing riveted and resistance spot welded aluminium sheets for the automotive industry. *Mater Des* 31(3):1457–1467. <https://doi.org/10.1016/j.matdes.2009.08.031>
- Briskham P, Blundell N, Han L, Hewitt R, Young K, Boomer D (2006) Comparison of self-pierce riveting, resistance spot welding and spot friction joining for aluminium automotive sheet. *Sae Sp* 2034:105
- Uhe B, Kuball C-M, Merklein M, Meschut G (2021) Strength of self-piercing riveted Joints with conventional Rivets and Rivets made of High Nitrogen Steel. Paper presented at ESAFORM 2021. 24th International Conference on Material Forming, Liège, Belgique. <https://doi.org/10.25518/esaform21.1911>
- Zhang C-Y, Gou R-B, Yu M, Zhang Y-J, Qiao Y-H, Fang S-P (2017) Mechanical and fatigue properties of self-piercing riveted joints in high-strength steel and aluminium alloy. *J Iron Steel Res Int* 24(2):214–221
- Sun X, Stephens E, Khaleel M (2007) Fatigue behaviors of self-piercing rivets joining similar and dissimilar sheet metals. *Int J Fatigue* 29(2):370–386. <https://doi.org/10.1016/j.ijfatigue.2006.02.054>
- Booth G, Olivier C, Westgate S, Liebrecht F et al (2000) Self-piercing riveted joints and resistance spot welded joints in steel and aluminium. *SAE Tech Pap*. <https://doi.org/10.4271/2000-01-2681>
- Li D (2017) Influence of aluminium sheet surface modification on the self-piercing riveting process and the joint static lap shear strength. *Int J Adv Manuf Technol* 93(5):2685–2695. <https://doi.org/10.1007/s00170-017-0710-6>
- Han L, Chrysanthou A (2008) Evaluation of quality and behaviour of self-piercing riveted aluminium to high strength low alloy sheets with different surface coatings. *Mater Des* 29(2):458–468. <https://doi.org/10.1016/j.matdes.2006.12.020>
- Uhe B, Kuball CM, Merklein M, Meschut G (2021) Influence of the rivet coating on the friction during self-piercing riveting. *Key Eng Mater* 883:11–18. <https://doi.org/10.4028/www.scientific.net/KEM.883.11>
- Huang L, Bonnen J, Lasecki J, Guo H, Su X (2016) Fatigue and fretting of mixed metal self-piercing riveted joint. *Int J Fatigue* 83:230–239. <https://doi.org/10.1016/j.ijfatigue.2015.10.018>
- Han L, Chrysanthou A, O'Sullivan JM (2006) Fretting behaviour of self-piercing riveted aluminium alloy joints under different interfacial conditions. *Mater Des* 27(3):200–208. <https://doi.org/10.1016/j.matdes.2004.10.014>
- Li D, Han L, Thornton M, Shergold M, Williams G (2014) The influence of fatigue on the stiffness and remaining static strength of self-piercing riveted aluminium joints. *Mater Des* 1980–2015(54):301–314
- Xu Y (2013) Effects of factors on physical attributes of self-piercing riveted joints. *Sci Technol Weld Joining* 11(6):666–671. <https://doi.org/10.1179/174329306x131866>
- Calabrese L, Proverbio E, Pollicino E, Galtieri G, Borsellino C (2014) Effect of galvanic corrosion on durability of aluminium/steel self-piercing rivet joints. *Corros Eng Sci Technol* 50(1):10–17. <https://doi.org/10.1179/1743278214y.0000000168>
- Janardhan G, Mukhopadhyay G, Kishore K, Dutta K (2020) Resistance spot welding of dissimilar interstitial-free and high-strength low-alloy steels. *J Mater Eng Perform* 29(5):3383–3394. <https://doi.org/10.1007/s11665-020-04857-z>
- Sun X, Stephens EV, Khaleel MA, Shao H, Kimchi M (2004) Resistance spot welding of aluminium alloy to steel with transition material - from process to performance—part I: experimental study. *Weld J-New York* 83:188–S
- Sawhill JM (1981) Spot weldability tests for high-strength steels. *SAE Trans* 90:1462–1472
- Han L, Chrysanthou A, Young KW (2007) Mechanical behaviour of self-piercing riveted multi-layer joints under different specimen configurations. *Mater Des* 28(7):2024–2033. <https://doi.org/10.1016/j.matdes.2006.06.015>
- Janardhan G, Kishore K, Mukhopadhyay G, Dutta K (2020) Fatigue properties of resistance spot welded dissimilar interstitial-free and high strength micro-alloyed steel sheets. *Met Mater Int* 27(9):3432–3448. <https://doi.org/10.1007/s12540-020-00678-w>
- Kishore K, Kumar P, Mukhopadhyay G (2021) Microstructure, tensile and fatigue behaviour of resistance spot welded zinc coated dual phase and interstitial free steel. *Met Mater Int*. <https://doi.org/10.1007/s12540-020-00939-8>
- Huang L, Shi Y, Guo H, Su X (2016) Fatigue behavior and life prediction of self-piercing riveted joint. *Int J Fatigue* 88:96–110. <https://doi.org/10.1016/j.ijfatigue.2016.03.015>
- Chen YK, Han L, Chrysanthou A, O'Sullivan JM (2003) Fretting wear in self-piercing riveted aluminium alloy sheet. *Wear* 255(7–12):1463–1470. [https://doi.org/10.1016/s0043-1648\(03\)00274-6](https://doi.org/10.1016/s0043-1648(03)00274-6)
- Zhao L et al (2017) Fretting behavior of self-piercing riveted joints in titanium sheet materials. *J Mater Process Technol* 249:246–254. <https://doi.org/10.1016/j.jmatprotec.2017.06.016>
- Zhao L, He X, Xing B, Lu Y, Gu F, Ball A (2015) Influence of sheet thickness on fatigue behavior and fretting of self-piercing riveted joints in aluminum alloy 5052. *Mater Des* 87:1010–1017. <https://doi.org/10.1016/j.matdes.2015.08.121>
- Han L, Chrysanthou A, Young KW, O'Sullivan JM (2006) Characterization of fretting fatigue in self-piercing riveted aluminium alloy sheets. *Fatigue Fract Eng Mater Struct* 29(8):646–654. <https://doi.org/10.1111/j.1460-2695.2006.01045.x>

35. He X, Deng C, Zhang X (2016) Fretting behavior of SPR Joining dissimilar sheets of titanium and copper alloys. *Metals*. <https://doi.org/10.3390/met6120312>
36. Rao HM, Kang J, Shi L, Sigler DR, Carlson BE (2018) Effect of specimen configuration on fatigue properties of dissimilar aluminum to steel resistance spot welds. *Int J Fatigue* 116:13–21. <https://doi.org/10.1016/j.ijfatigue.2018.06.009>
37. Khan MS, Bhole SD, Chen DL, Biro E, Boudreau G, van Deventer J (2013) Welding behaviour, microstructure and mechanical properties of dissimilar resistance spot welds between galvanized HSLA350 and DP600 steels. *Sci Technol Weld Joining* 14(7):616–625. <https://doi.org/10.1179/136217109x12464549883295>
38. Kaneko N, Sasaki T (2014) Ultrasonic spot welding of galvanized steel sheet. *Adv Mater Res* 922:332–337. <https://doi.org/10.4028/www.scientific.net/AMR.922.332>

Publisher's Note Springer Nature remains neutral with regard to jurisdictional claims in published maps and institutional affiliations.

Springer Nature or its licensor holds exclusive rights to this article under a publishing agreement with the author(s) or other rightsholder(s); author self-archiving of the accepted manuscript version of this article is solely governed by the terms of such publishing agreement and applicable law.